Time-Resolved Reversal of Spin-Transfer Switching in a Nanomagnet

R. H. Koch,[1] J. A. Katine,[2,*] and J. Z. Sun[1]

[1]*IBM T. J. Watson Research Center, P.O. Box 218, Yorktown Heights, New York 10598, USA*
[2]*IBM Almaden Research Center, 650 Harry Road, San Jose, California 95120, USA*

(Received 12 June 2003; published 26 February 2004)

Time-resolved measurements of spin-transfer-induced (STI) magnetization reversal were made in current-perpendicular spin-valve nanomagnetic junctions subject to a pulsed current bias. These results can be understood within the framework of a Landau-Lifshitz-Gilbert equation that includes STI corrections and a Langevin random field for finite temperature. Comparison of these measurements with model calculations demonstrates that spin-transfer induced excitation is responsible for the observed magnetic reversal in these samples.

DOI: 10.1103/PhysRevLett.92.088302 PACS numbers: 85.70.Kh, 73.63.–b, 75.40.Gb, 85.75.–d

Nonequilibrium spin-transfer-induced [1–8] (STI) magnetization reversal is a phenomenon observed only in small spin-valve structures typically less than 0.1 μm in size. It reveals a new type of interaction between magnetization and a spin-polarized transport current. To understand the nature of these interactions and to confirm a modified Landau-Lifshitz-Gilbert (LLG) equation description, it is important to experimentally examine STI reversal including the effects of temperature. Experiments measuring dc (or quasi-dc) transport [9,10] as well as microwave emission [11–13] already begin to address this question, but complications associated with accounting for finite temperature effects in previous experiments make time-resolved reversal experiments complimentary and revealing.

Here we describe an experiment that measures the magnetoresistance response of a spin-valve junction in response to spin-transfer-induced reversal. The experiment demonstrates the combined effect of spin transfer and thermal activation on the reversal process of a nanomagnet. It gives an experimental assessment of the reversal speed and its dependence on driving current amplitude. Our measurements confirm the subcritical current thermal-activation mechanism as was previously reported by Albert *et al.* [9]. In addition our data reveal for the first time a supercritical region where a linear dependence of the switching speed on current amplitude is seen. This is a unique attribute of the spin-transfer process as it reflects angular momentum conservation.

The low impedance and small output signal in these devices make high-speed transport measurement nontrivial. All lithographically fabricated devices for observing this effect are of the current-perpendicular (CPP) spin-valve type, with low junction resistance (about 1–5 Ω), and small magnetoresistance (MR) changes (around 3%–5%). The resulting MR signal is small, typically <1 mV. Dynamic calculations (see, for example, Ref. [8]) give the generic time scale of the reversal to be around $(2\pi M_s)\gamma$, where $\gamma = 2\mu_B/\hbar$ is the gyromagnetic ratio, and M_s is the saturation magnetization of the thin-film nanomagnet. This places the zero-temperature switching time on the order of 1–10 ns.

CPP junctions with a Co/Cu/Co stack are used. Junctions are fabricated using electron beam lithography, either through a direct etch process similar to that in [7], or using a nanostencil substrate [14]. The junction reported here is designed to be about 0.05×0.10 μm^2 in size, and the free-layer cobalt is 30 Å thick. All measurements were performed at ambient temperature. The current-voltage (IV) curve was measured using a pair of Agilent 3458 voltmeters. Each IV curve is taken in about 100 sec. Figure 1(a) is a plot of the calculated dynamic resistance of a typical sample. The average resistance for this sample was 3.7 Ω and the MR is about 4%. Hence,

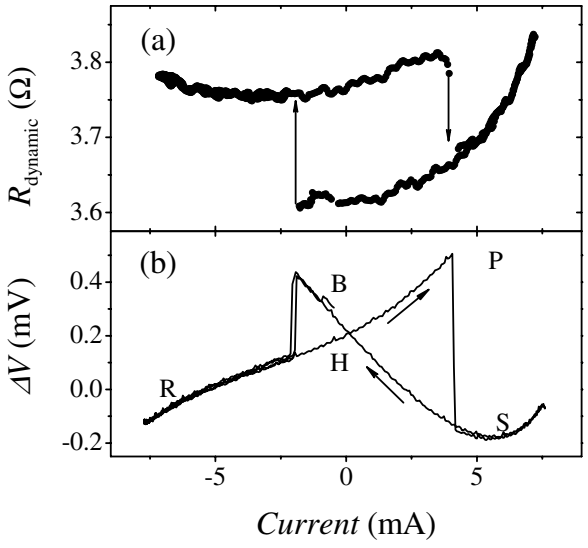

FIG. 1. (a) The dc response of a sample CPP spin valve under spin-polarized current injection showing the typical spin-current-induced magnetic switch. The junction shown here is about 50×100 nm^2 in size. (b) The difference between the measured IV curve and a straight line. The five points correspond to "H" = home, "B" = background, "P" = pulsed, "S" = switched, and "R" = reset.

 0031-9007/04/92(8)/088302(4)$22.50

the common mode signal is 25 times larger than the magnetoresistance signal.

A special pulse sequence was used. Figure 1(b) plots the difference between the measured voltage and a straight line vs the measured current. The measurement of the reversal time is done by alternately applying two pulse sequences, the "signal" and the "background" sequence. The sample is dc biased at the current that corresponds to points H (home) or B (background). For the signal sequence, a 1 μs long pulse is applied to place the sample at point R (reset). This forces the sample to be at point H after the pulse is removed. Second, a 300 (or sometimes a 30) ns pulse of varying amplitude is applied to metastably place the sample at point P (pulse). If the pulse is long and big enough, the sample will switch to point S (switched). During this sequence, the voltage across the sample is recorded using the Tektronix TDS6604 oscilloscope. The oscilloscope has a bandwidth of 6 GHz. The background sequence is taken in exactly the same manner as the signal sequence, except that the reset pulse is omitted. When the sample is current pulsed to be close to or always switching, the lack of a reset pulse assures that the sample is moving from point S to point B during the background sequence. The difference between the average voltages recorded between the two pulse sequences represents the magnetization reversal when the sample is biased between points P and S. We typically average about 10 000 traces in groups of 500 signal and background traces. During any one pulse realization, the sample will reverse at some point in time at a time scale much less than 300 ns. The measured results reflect the probability of being switched as a function of time averaged over many pulses.

Figure 2 plots the magnetization reversal time as a function of the pulsed current. We have measured about a hundred of these types of curves on over 20 samples. We estimate that the temperature rise of the sample from Joule heating during the measurement is less than 20 K. The baseline of the switched state is not completely flat because of the ac coupling used during the measurement. The fine ripple on the traces is coherent noise from the measurement system.

A switching time τ can be extracted from data such as shown in Fig. 2. A model-independent way is to extract a time necessary for data in Fig. 2 to decay a given percentage. Alternatively, it can be obtained from the data by fitting each trace to an exponential decay and extracting the decay constant. The dependence of τ_{decay} on pulsed bias current obtained using an exponential fit is shown in Fig. 3.

Two points are noted for the data shown in Fig. 3. First, at the high-speed limit, the dependence of τ^{-1} on bias current I is linear. Second, in the subthreshold, large-τ regime, this linearity gives way to a curved onset. We show below that the linear τ^{-1} vs I dependence stems from spin-transfer angular momentum conservation, and the curved onset relates to thermal activation. Both can be

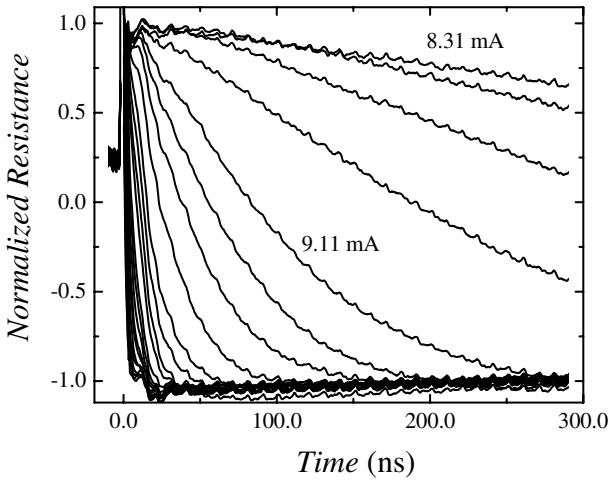

FIG. 2. A set of measured amplitude-dependent reversal traces. The response is normalized to vary from 1 to -1, which corresponds to a change in ΔR of 0.1 Ω. The pulse current values are uniformly spaced and vary from 8.31 to 12.71 mA.

adequately described by the spin-transfer dynamics with thermal noise. In addition, the threshold current observed in Fig. 3 is about 11 mA for the threshold corresponding to the right-side step of Fig. 1 which reads only about 4.5 mA. The difference between these two values lies in the vastly different time scales of the two measurements.

The dynamics of magnetization reversal have been described using the LLG equation [15] modified to include the spin-transfer excitation [1–8]. In the simplest limit, consider a monodomain nanomagnet with a magnetic moment $\mathbf{m}$: a charge current I spin polarized in the direction $\mathbf{n}_s$ and with a spin-polarization factor η passes through the nanomagnet, depositing a torque of $\mathbf{\Gamma} = -(\eta\hbar/2em^2)I(\mathbf{n}_s \times \mathbf{m}) \times \mathbf{m}$. The modified LLG equation can be written as

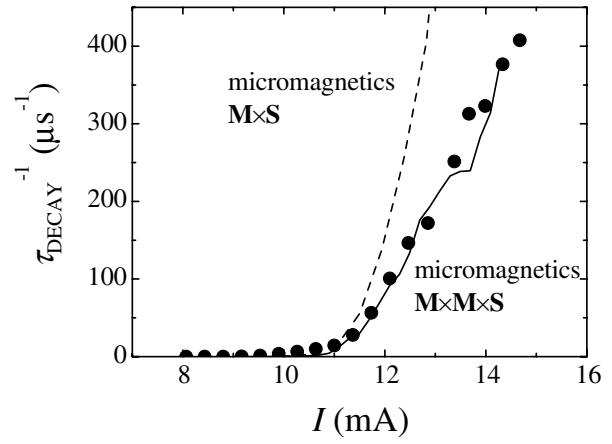

FIG. 3. The dots plot the current dependence of the experimentally measured reversal rate $1/\tau_{\mathrm{decay}}$, extracted from data as shown in Fig. 2. The linear intercept along the I axis gives the zero-temperature threshold current I_{c0}. The two lines indicate the results of different types of micromagnetic models of the reversal rate.

$$\left(\frac{1}{\gamma}\right)\frac{d\mathbf{m}}{dt} = \mathbf{m}\times\left[\mathbf{H} - \left(\frac{\alpha}{m}\right)\mathbf{m}\times(\mathbf{H}+\mathbf{H}_s)\right], \quad (1)$$

where $\gamma = 2\mu_B/\hbar$ is the gyromagnetic ratio, and $\mathbf{H}_s = (\eta I\hbar/2em\alpha)\mathbf{n}_s$ represents the contribution from spin transfer. Should there be other features in the potential energy landscape, the first term of $\mathbf{m}\times\mathbf{H}$ in Eq. (1) can be replaced by the energy function in the form of [8] $\mathbf{m}\times\mathbf{H}\rightarrow -\mathbf{n}_m\times\nabla U$, where U is the full energy potential the magnetic moment experiences.

Equation (1) in the presence of both uniaxial and easy-plane anisotropy fields of H_k and $4\pi M_s$ gives approximately a linear dependence between the switching time τ^{-1} and the bias current I. Similar to the results shown in Ref. [8],

$$\tau^{-1} \approx \frac{\alpha\gamma}{\ln(\pi/2\theta_0)}(H + H_k + 2\pi M_s)[(I/I_{c0}) - 1]$$
$$= \frac{\eta(\mu_B/e)}{m\ln(\pi/2\theta_0)}(I - I_{c0}), \qquad (I > I_{c0}). \quad (2)$$

Here θ_0 is the initial angular deviation of the magnetic moment from its easy axis, and $I_{c0} = (1/\eta)(2e/\hbar)\times\alpha m(H + H_k + 2\pi M_s)$ is the zero-temperature threshold current for spin-transfer-induced magnetic reversal. This result reflects conservation of angular momentum and is the origin of the linear slope at high bias current observed in Fig. 3.

The effect of a finite temperature is twofold. First, it creates a thermally distributed initial value θ_0. This for $I \gg I_{c0}$ has the effect of giving a thermally distributed switching time τ, the ensemble average of which preserves the linear dependence of τ^{-1} in $(I - I_{c0})$ but rescales the prefactor. Second, in the subcritical region $I < I_{c0}$, finite temperature gives a finite probability for thermally activated switching, which requires a LLG equation that includes thermal perturbation.

To describe the effect of temperature, one follows the approach of Brown [16] and Grinstein *et al.* [17] in adding a Langevin random field $\mathbf{H}_L$ to the magnetic field $\mathbf{H}$. The Langevin field $\mathbf{H}_L$ relates to the system temperature as $H_{L,i} = \sqrt{2\alpha k_B T/\gamma m}I_{\mathrm{ran},i}(t)$ $(i = x, y, z)$, where $I_{\mathrm{ran}}(t)$ is a Gaussian random function with the first two moments of $\langle I_{\mathrm{ran}}(t)\rangle = 0$ and $\langle I^2_{\mathrm{ran}}(t)\rangle = 1$. The x, y, and z components each have their own uncorrelated $I_{\mathrm{ran}}(t)$. Equation (1) can then be discretized and numerically integrated.

A special case of Eq. (1) is when $\mathbf{H}$ and $\mathbf{H}_s$ are collinear, that is, $\mathbf{H} = H\mathbf{n}_s$, and $\mathbf{H}_s = H_s\mathbf{n}_s$. In this case, one can write Eq. (1) as

$$\left(\frac{1}{\gamma}\right)\frac{d\mathbf{m}}{dt} = \mathbf{m}\times\left[\mathbf{H} - \left(\frac{\tilde{\alpha}}{m}\right)\mathbf{m}\times\mathbf{H}\right], \quad (3)$$

where a new effective LLG damping coefficient $\tilde{\alpha}$ is introduced so that $\tilde{\alpha} = (1 + H_s/H)\alpha$, which explicitly reveals the role of spin-transfer excitation H_s: it modifies the effective damping, and when $H_s/H < -1$, $\tilde{\alpha} < 0$, the system amplifies, rather than damps, any disturbance from equilibrium.

Furthermore, if one introduces a fictitious temperature $\tilde{T}$ such that $\tilde{\alpha}\tilde{T} = \alpha T$, one can rewrite Eq. (3) with a consistent set of parameters both for the Langevin term and for the effective damping:

$$\begin{cases} \left(\frac{1}{\gamma}\right)\frac{d\mathbf{m}}{dt} = \mathbf{m}\times[(\mathbf{H}+\mathbf{H}_L) - \left(\frac{\tilde{\alpha}}{m}\right)\mathbf{m}\times\mathbf{H}], \\ H_{L,i} = \sqrt{2\tilde{\alpha}k_B\tilde{T}/\gamma m}I_{\mathrm{ran},i}, \qquad (i = x, y, z). \end{cases} \quad (4)$$

Equation (4) is equivalent to having a nanomagnet with damping $\tilde{\alpha}$ and at temperature $\tilde{T}$, which can be translated into a simple thermal-activation picture of $\tau = \tau_0\exp(E/k_B\tilde{T})$. Here τ is the thermal-activation lifetime, τ_0 is the inverse of the attempt frequency of the nanomagnet, and E is the actual barrier height of the nanomagnet as determined by its size, shape, applied field strength, and intrinsic magnetic anisotropy environment. For a thin-film nanomagnet with uniaxial and easy-plane anisotropy only, one may write $E = E_0(1 + h_a)^2$, where $h_a = H/H_k$ with H_k being the easy-axis magnetic anisotropy field as determined by the shape anisotropy of the nanomagnet, and $E_0 = (1/2)mH_k$.

The lifetime for activated reversal is controlled by the spin-transfer current I through $\tilde{T} = T/[1 + I(\eta\hbar/2em\alpha H)]$. This gives an effective reversal threshold current of $I_c = (1/\eta)(2e/\hbar)\alpha(mH)\times[1 - (k_BT/E)\ln(\tau/\tau_0)]$. Comparing this with the zero-temperature spin-transfer threshold current of $I_{c0} = (1/\eta)(2e/\hbar)\alpha m(H + H_k + 2\pi M_s)$ derived in Ref. [8], one sees that the effect of thermal activation is to rescale the threshold current by a factor of $[1 - (k_BT/E)\times\ln(\tau/\tau_0)]$. In general one may write $I_c = I_{c0}[1 - (k_BT/E)\ln(\tau/\tau_0)]$. Therefore, in the thermal-activation region $(I \ll I_{c0})$:

$$\tau^{-1} = \tau_0^{-1}\exp[-\Delta_0(1 + h_a)^2(1 - I/I_{c0})] \quad (5)$$

in which $\Delta_0 = E_0/k_BT$. This result agrees with the general theoretical conclusion obtained by Li and Zhang [18] using non-conserving-force thermodynamics and is also consistent with the current dependence observed by Urazhdin *et al.* [10].

Equations (2) and (5) describe the two asymptotic limits of τ^{-1} vs I for $I \gg I_{c0}$ and $I \ll I_{c0}$, respectively. They can be readily compared with data such as those shown in Fig. 3.

In between the two asymptotic limits of Eqs. (2) and (5), the dependence of τ^{-1} on bias current I can be calculated by numerically integrating Eq. (4). There are three essential adjustable parameters for determining the numerical calculation: the LLG damping coefficient α, the spin-polarization factor η, and the barrier-to-temperature ratio $\Delta = \Delta_0(1 + h_a)^2(1 - I/I_{c0})$.

In Fig. 4 the experimental switching time τ^{-1} is compared with a monodomain calculation. A set of numerically calculated switching times for such a monodomain nanomagnet at different bias-current levels are shown as

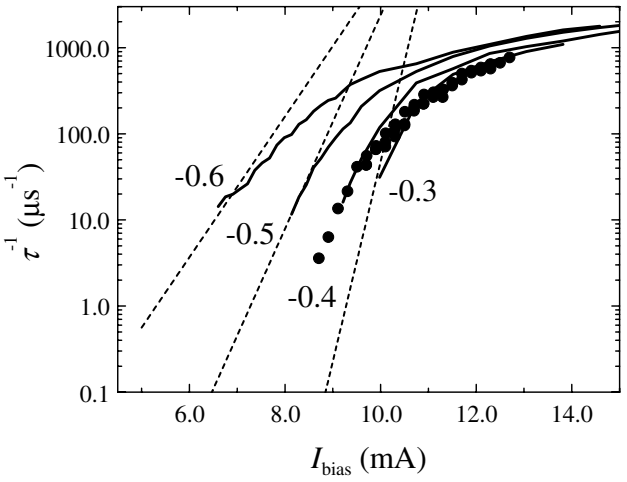

FIG. 4. Comparing model calculation with experiment. Points are data. Model calculations assume a junction size of $0.05 \times 0.10\ \mu\text{m}^2 \times 30$ Å, with $M_s \approx 1440$ emu/cm^3 for cobalt; $\alpha = 0.0326$, $T = 300$ K, $\eta = 0.5$. Thick solid lines are numerical simulation results at different values of h_a as indicated on the plot. Dashed lines are from the analytical expression Eq. (5) for subcritical thermal activation using $h_a = -0.3$, -0.5, and -0.6, respectively.

solid lines in Fig. 4. In the set of numerical simulations presented in Fig. 4, we computed results for different Δ by varying the values of h_a, while keeping the zero-field barrier height $E_0 = 120 k_B T$ as one would expect from the shape anisotropy of a single cobalt thin-film nanomagnet of the size $0.05 \times 0.10\ \mu\text{m}^2$ by 30 Å thick. From data shown in Fig. 4, the experimental data agree best with numerical results with h_a between -0.3 and -0.4.

A similar conclusion is reached by comparing the subcritical thermally activated switching using Eq. (5). Assume $\tau_0 = 10^{-9}$ sec, $\tau = 10^{-2}$ sec for dc IV measurements; from the intercept of the linear portion of τ^{-1} such as shown in Fig. 3 we have the threshold $I_{c0} \sim 10$ mA, and from Fig. 1, the dc threshold is $I \sim 4.5$ mA. These and Eq. (5) give $\Delta_0(1 + h_a)^2 = 29$. For $\Delta_0 = 120$, this gives $h_a \approx -0.5$, close to the numerical simulation result.

Further numerical work involves a full micromagnetics simulation including the STI excitation $\mathbf{M} \times \mathbf{M} \times \mathbf{S}$, and perhaps even with the possibility of including an STI exchange field term. Figure 3 shows two types of predictions for the $1/\tau_{\text{decay}}$ or the reversal rate at $T = 300$ K. Here we have added a term to the standard micromagnetic LLG equation (in MKS units) of the form $d\mathbf{M}/dt = -(\gamma\mu_0/|\mathbf{M}|)\mathbf{M} \times \mathbf{M} \times \mathbf{S}$ [19]. Also we have simulated the STI exchange term, i.e., the $\mathbf{M} \times \mathbf{S}$ term. In this case we have added a magnetic field term of the form $\mathbf{S} \equiv \lambda J \mathbf{n}_s$ to the usual LLG equation. This is the effective magnetic field from the STI exchange interaction, and it appears in both the $\mathbf{M} \times \mathbf{H}$ and the $\mathbf{M} \times \mathbf{M} \times \mathbf{H}$ terms in the LLG equation. To properly predict the finite temperature behavior of the sample, we have used the methods described in Ref. [17]. The data plotted in Fig. 3 match exactly the conditions of the experiment, including simulating the reversal hundreds of times to extract the average probability of reversal vs time. Here we used the parameter λ as adjustable to account for the unknown value of the spin polarizations and the angle dependent spin transfer. To that extent, we have adjusted λ so that the simulated zero-temperature critical current matches the measured value. In these simulations we have used values of λ of 5 and 13 nm for the $\mathbf{M} \times \mathbf{M} \times \mathbf{S}$ and $\mathbf{M} \times \mathbf{S}$ terms, respectively. So the comparison between the measurements and the simulations is to be made in the slope of the curves. It is clear from the figure that the predictions using the $\mathbf{M} \times \mathbf{M} \times \mathbf{S}$ term fits the measured data well and the $\mathbf{M} \times \mathbf{S}$ term does not.

We thank R. A. Carruthers, J. M. E. Harper, M. J. Rooks, and C. T. Black for assistance.

*Present address: Hitachi San Jose Research Center, 650 Harry Road, San Jose, CA 95120, USA.

[1] L. Berger, J. Appl. Phys. **49**, 2156 (1978).
[2] J. C. Slonczewski, J. Magn. Magn. Mater. **159**, L1 (1996).
[3] Y. B. Bazaliy, B. A. Jones, and S.-C. Zhang, Phys. Rev. B **57**, R3213 (1998).
[4] M. Tsoi, A. G. M. Jansen, J. Bass, W.-C. Chiang, M. Seck, V. Tsoi, and P. Wyder, Phys. Rev. Lett. **80**, 4281 (1998).
[5] E. B. Myers, D. C. Ralph, J. A. Katine, R. N. Louie, and R. A. Buhrman, Science **285**, 867 (1999).
[6] J. Z. Sun, J. Magn. Magn. Mater. **202**, 157 (1999).
[7] J. A. Katine, F. J. Albert, R. A. Buhrman, E. B. Myers, and D. C. Ralph, Phys. Rev. Lett. **84**, 3149 (2000).
[8] J. Z. Sun, Phys. Rev. B **62**, 570 (2000).
[9] F. J. Albert, N. C. Emley, E. B. Myers, D. C. Ralph, and R. A. Buhrman, Phys. Rev. Lett. **89**, 226802 (2003).
[10] S. Urazhdin, N. O. Birge, W. P. Pratt, Jr., and J. Bass, Phys. Rev. Lett. **91**, 146803 (2003).
[11] M. Tsoi, A. G. M. Jansen, J. Bass, W.-C. Chiang, V. Tsoi, and P. Wyder, Nature (London) **406**, 46 (2002).
[12] S. I. Kiselev, J. C. Sankey, I. N. Krivorotov, N. C. Emley, R. J. Schoelkopf, R. A. Buhrman, and D. C. Ralph, Nature (London) **425**, 380 (2003).
[13] A. V. Nazarov, H. S. Cho, J. Nowak, S. Stokes, and N. Tabat, Appl. Phys. Lett. **81**, 4559 (2002).
[14] J. Z. Sun, D. J. Monsma, M. J. Rooks, and R. H. Koch, Appl. Phys. Lett. **81**, 2202 (2002).
[15] E. M. Lifshitz and L. P. Pitaevskii, *Statistical Physics* (A. Wheaton & Co. Ltd., Exeter, 1981), Pt. 2, Chap. 7, p. 285.
[16] W. F. Brown, Phys. Rev. **130**, 1677 (1963).
[17] G. Grinstein and R. H. Koch, Phys. Rev. Lett. **90**, 207201 (2003).
[18] Z. Li and S. Zhang, cond-mat/0302339.
[19] Here $\mathbf{M}$ and $\mathbf{S}$ are the continuous-medium equivalents (in MKS units) of $\mathbf{m}$ and $\mathbf{H}_s$ (in cgs units). The magnitude of $\mathbf{S}$ is proportional to the current density J in the form of $\mathbf{S} \equiv \lambda J \mathbf{n}_s$ in MKS units. It is the continuous-medium equivalent of $\mathbf{H}_s = (\eta I \hbar / 2em\alpha)\mathbf{n}_s$.